Using Sodium Cation Organization To Study the Phase Behavior of Bicelle Solutions

S. Vyas, A. J. Weekley, B. K. Tenn, J. C. Flinders, T. Dieckmann, and M. P. Augustine*

Department of Chemistry, One Shields Avenue, University of California, Davis, California 95616

Received: December 16, 2002; In Final Form: June 16, 2003

The ^{23}Na nuclear magnetic resonance (NMR) spectra for NaCl dissolved in the nematic phase of dimyristoyl−phosphatidylcholine (DMPC)/dihexanoyl−phosphatidylcholine (DHPC) bicelle solutions at 34 °C display line splittings consistent with the quadrupolar satellite transitions for the $I = {}^3/_2$ ^{23}Na nucleus. At temperatures exceeding 40 °C additional residual ^{23}Na satellite transition lines develop, suggesting that a new ordered phase similar to pure DMPC is present.

Introduction

The importance of biomolecular shape, size, and charge in regulating life has generated substantial interest in the development of new techniques capable of retrieving secondary, tertiary, and quarternary chemical structure with unprecedented resolution and fidelity. One particularly important approach involves using molecular constructs such as aqueous phase biologically friendly liquid crystal solvents such as the magnetically orientable Pf1 bacteriophage,[1] bacteriorhodopsin purple membranes,[2,3] or the phospholipid bicelles[4−6] to interrupt the isotropic tumbling of solutes and hence reintroduce chemical structure dependent features to the NMR spectrum of the solute. Of these media, the phospholipid bicelles are attractive due to their surface charge and ability to behave as cell membrane mimics.[7] It is known that careful control of the pH, ionic strength, and concentration of the DMPC and DHPC molecular building blocks in the bicelle in molar ratios q = DMPC/DHPC between 3 and 3.5 can lead to well-defined homogeneous liquid crystalline phases over 10−20 °C temperature ranges.[8,9] In addition, the highly anisotropic magnetic susceptibility of these disklike phospholipid clusters is known to orient the bicelles edge-on in the external magnetic field used to observe magnetic resonance.[8,9]

An empirical formula provided by Vold et al.[9] allows the calculation of the average dimensions of a bicelle, given the molar ratio q and the 2 nm length of the DHPC molecule in the binary phospholipid mixture. As an example, a DMPC/DHPC phospholipid solution in liquid water with $q = 3.25$ produces approximately 26 nm diameter bicelles. Each of these disks is composed of approximately 10^4 molecules, of which 76% are DMPC and the remaining are DHPC. Considering that the positive charge for each of these zwitterionic phospholipid molecules is in contact with solution and using the total surface area of the bicelle, the charge density on the surface is $\sigma = 41$ μC/cm^2. Given this unusually high surface charge density, one would expect that smaller counterions would be nonuniformly distributed around the bicelle in solution. In fact, the polyelectrolyte behavior of the bicelles should generate a corresponding ion atmosphere and hence a nonzero electric potential, electric field, and electric field gradient near the bicelle surface. It has been long established that the NMR spectra of quadrupolar ions are sensitive to electric field gradients in an anisotropic medium like aqueous phase lamellar liquid crystals.[10] A number of models exist that describe residual quadrupolar effects in these liquid crystalline systems,[10,11] and it is anticipated that solutions to the Poisson−Boltzmann equation that have been successfully applied to the rodlike polyelectrolytes[12−14] can be generalized to apply here in the case of the oblate spheroidal phospholipid bicelles.

This paper presents the results of probing the electric field gradients near the surface of a DMPC/DHPC bicelle using ^{23}Na NMR. The results demonstrate that the quadrupolar ions having $I > {}^1/_2$ are excellent probes for the asymmetric bicelle medium and its associated constitutional changes with temperature. The line splittings observed in solution are compared to calculated frequencies, and useful conclusions about the liquid crystalline morphology are gleaned. Finally, these conclusions are tested by comparison to ^{23}Na NMR spectra in pure DMPC solutions where bicelle formation is not a possibility and the observables appear to be governed by the formation of bilayers.

Experimental Section

Phospholipids were purchased as binary mixtures of DHPC and DMPC ($q = 3.25$) from Avanti Polar Lipids (Alabaster, AL), and the bicelles were made according to the following commercial procedure. The lipid mixture was first dissolved in a pH = 6.6 solution containing 10 mM phosphate buffer, 0.15 mM sodium azide, 93% H_2O, and 7% D_2O (99.9%). Following a brief period of vortexing, the sample was heated to 40 °C for 20 min and then cooled to 4 °C to ensure rapid hydration. After repeating the hydration process, sodium chloride obtained from Aldrich chemical company was added at a concentration of 30 mM. All NMR spectra for ^{23}Na at a Larmor frequency of 156.26 MHz were obtained using a Bruker DRX-600 NMR spectrometer operating at a magnetic field strength of 13.9 T. In all variable temperature measurements, care was taken to ensure that a stable equilibrium temperature was established by waiting at least 10 min at each temperature before data acquisition. All data processing and spectral analysis were accomplished using Matlab.

The NMR Spectrum

The ^{23}Na NMR spectrum for NaCl dissolved in water contains just one peak reflecting an average electric field gradient $\langle \nabla^2 V \rangle$ of zero. Here all three of the $|\Delta m| = 1$ transitions in the $I = {}^3/_2$

* To whom correspondence should be addressed. E-mail address: augustin@chem.ucdavis.edu.

10.1021/jp022606a CCC: $25.00
Published on Web 09/09/2003

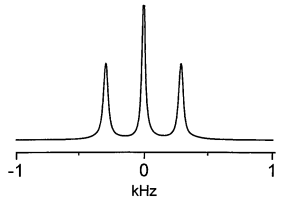

Figure 1. ^{23}Na NMR spectrum for 30 mM NaCl dissolved in a 40% w/v solution of DMPC/DHPC ($q = 3.25$) at 34 °C.

^{23}Na nucleus are degenerate in energy and thus overlap in the ^{23}Na NMR spectrum. The situation is different for a sodium cation in a partially oriented charged medium because the interaction of the nuclear quadrupole moment Q with a nonzero electric field gradient separates the $m = -3/2 \leftrightarrow m = -1/2$ and $m = +3/2 \leftrightarrow m = +1/2$ satellite transitions from the $m = -1/2 \leftrightarrow m = +1/2$ center band. The frequency difference between the satellite transitions can be described to first order as

$$\Delta = \frac{eQ}{h}\langle\nabla^2 V\rangle \tag{1}$$

where e is the fundamental electrostatic charge and h is Planck's constant. The ^{23}Na NMR spectrum for an ion in a charged oriented phase therefore has three lines separated by $\Delta/2$ and in a $^3/_4$:1:$^3/_4$ intensity ratio. The satellite transition splitting Δ can be used to extract details concerning the electrical properties of the aligned liquid crystal via its dependence on the average $\langle\nabla^2 V\rangle$. In the special case of both Pf1 and bicelle solutions where the building blocks of the liquid crystal are well defined, are at least 3 orders of magnitude larger than a monovalent ion, and have thousands of ion binding sites, it is reasonable to consider the solutions as being composed of uniformly charged objects—rods and disks, respectively. In the classical limit one solves the Poisson−Boltzmann equation for the potential $V(\tau)$ in three dimensions τ and uses the ion charge distribution $\rho(r,\theta,\phi)$ to calculate the steady-state average of the field gradient $\langle\nabla^2 V\rangle$ around the construct. This approach for calculating $\langle\nabla^2 V\rangle$ of course breaks down when the molecular building blocks of the liquid crystal are not well-defined, are small in comparison to the ionic radius of the NMR probe nucleus, or have low charge. In this case a chemical exchange between a binding site with a large $\nabla^2 V(\tau)$ value and a site with $\nabla^2 V(\tau) = 0$ is considered to determine the observed splitting Δ. Separation of the two cases can be somewhat tedious and even impossible. However, the classical limit involving large well-defined objects typically displays $I = 3/2$ NMR spectra with a well-resolved splitting Δ and narrow lines. On the other hand the ^{23}Na NMR spectra for less well-defined phases or those involving small molecular building blocks will be less resolved and may even involve powder pattern line shapes.

The Bicelle Phase

The ^{23}Na NMR spectrum in Figure 1 corresponds to a 40% w/v, $q = 3.25$ DMPC/DHPC solution at 34 °C. The three equally spaced resonances in roughly a $^3/_4$:1:$^3/_4$ integrated intensity ratio can be used to extract a $\Delta = 600$ Hz value for the residual quadrupolar splitting. It is well-known that the binary lipid mixture goes through a series of structural transitions as a function of temperature during the formation of a homogeneous bicelle solution. For the 40% w/v $q = 3.25$ DMPC/DHPC mixture considered here, the liquid crystalline bicelle phase has been shown by ^{31}P and ^{2}H NMR of labeled phospholipids[9,15] and by ^{2}H NMR of D_2O[8] to persist between roughly 27 and 40 °C. It is believed that in this temperature range the DMPC and DHPC molecules begin to aggregate into tiny disk-shaped assemblies that ultimately magnetically align.

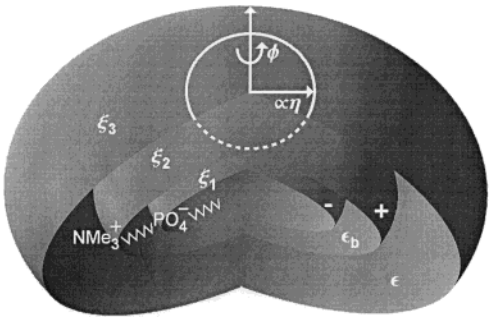

Figure 2. Model of the phospholipid bicelle. The zwitterionic phospholipid headgroups on the bicelle surface are considered as concentric charged oblate ellipsoids enclosing a region with dielectric constant ϵ_b/ϵ_0. The inner PO_4^- surface is defined by ξ_1, and the outer NMe_3^+ surface is defined by ξ_2. The interbicelle region is filled with water and ions having a dielectric constant of ϵ/ϵ_0 and the bicelle separation of $2d = 10$ nm can be used to define an outer cell at ξ_3, where the electric field drops to zero.

A combination of these facts with the well-resolved spectrum in Figure 1 suggests that the splitting Δ can be calculated by modeling the zwitterionic surface of the bicelles as an oblate spheroidal surface in solution. In analogy to the rodlike polyelectrolytes where the construction of a cell around a charged cylinder has been shown to predict both the nuclear spin relaxation properties[12] and residual quadrupolar splitting of ^{23}Na in solution,[14] a similar oblate spheroidal surface adapted to the bicelle symmetry can be used to define a cell around a chosen bicelle. As in any coordinate system, there are three variables describing a location in space. In terms of a point on the oblate spheroid surface a distance r_1 and r_2 from the two foci of the ellipse used to construct the spheroidal surface and separated by the distance a, the latitude and expansion factor are $\eta = (r_1 - r_2)/a$ and $\xi = (r_1 + r_2)/a$, respectively.[16] These two variables in addition to rotation about the major symmetry axis of the oblate spheroid ϕ are included in Figure 2. Because the bicelles form a liquid crystalline phase, it is reasonable to assume that the disks are separated by a distance 2d and that the surface of the bicelle behaves like an unreactive electrode in solution. The simplest approach to calculating Δ or equivalently the average $\langle\nabla^2 V\rangle$ involves determining the electric potential $V(\xi,\eta,\phi)$ and the positive $\rho_+(\xi,\eta,\phi)$ and negative $\rho_-(\xi,\eta,\phi)$ ion distributions in the double layer or ion atmosphere around the bicelle using electrical boundary layer theory. Unfortunately the Debye−Hückel approximation cannot be used in this case due to a combination of the high bicelle surface charge and the anticipated high dielectric constant ($\epsilon/\epsilon_o = 80$) of the water between bicelles. The calculation of $V(\xi,\eta,\phi)$ proceeds in direct analogy to Engström et al.,[17] who considered the effect of cationic plates formed by surfactants in solution. The model bicelle enclosed within an oblate spheroidal shell is shown in Figure 2. The distance of closest approach between the positive and negative surface is set by the $l = 10$ Å separation of the PO_4^- anion and NMe_3^+ cation constituents of the zwitterionic polar headgroup in DMPC, as measured by X-ray diffraction.[18] The bicelles are separated by a distance $2d$ and have a surface potential set by the electric field developed between the uniformly charged PO_4^- and NMe_3^+ headgroup ionic surfaces within a bicelle, as shown in Figure 2. These observations, coupled with the fact that the electric field at the midpoint between bicelles must drop to zero, imply that the potential is only a function of the expansion factor ξ or,

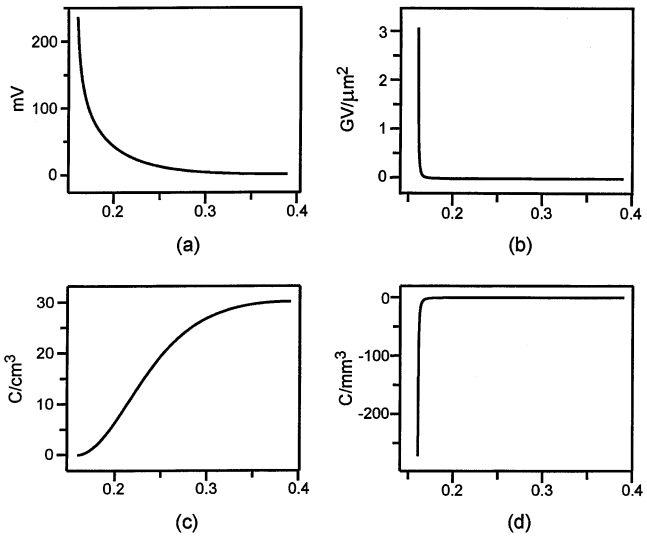

Figure 3. Plots of the numerical solution to the Poisson−Boltzmann equation shown in eq 2 for $V(\xi)$, $\nabla^2V(\xi)$, $\rho_+(\xi)$, and $\rho_-(\xi)$ in (a)−(d), respectively. All of these curves are appropriate for the same 40% w/v electroneutral solution of 26 nm diameter bicelles with 30 mM added NaCl and $\epsilon/\epsilon_0 = 80$.

equivalently, the potential drops from the bicelle surface in a manner consistent with oblate spheroidal shells. The 26 nm diameter 4 nm thick bicelle dimension can be used to calculate that the foci of the bicelle are separated by $a = 12.65$ nm and that the expansion factor ξ defining the bicelle or NMe_3^+ surface is $\xi_2 = 0.16$.[16] The $l = 10$ Å separation between the PO_4^- and NMe_3^+ surfaces of the bicelle can be used to define the expansion factor for the PO_4^- surface as $\xi_1 = 0.08$ whereas the $2d = 10$ nm bicelle separation yields $\xi_3 = 0.39$. Given that the region between bicelles $\xi_2 < \xi < \xi_3$ is filled with both water and equivalent amounts of positive and negative free ions, the one-dimensional Poisson−Boltzmann equation appropriate for this situation is

$$\frac{\mathrm{d}}{\mathrm{d}\xi}(\xi^2+1)\frac{\mathrm{d}}{\mathrm{d}\xi}V(\xi) = \frac{2eN}{\epsilon}\sinh\left(\frac{eV(\xi)}{kT}\right) \qquad (2)$$

where $\rho(\xi) = \rho_+(\xi) + \rho_-(\xi) = -2eN\sinh(eV(\xi)/kT)$ is the total free charge density, N is the number density of monovalent ions in solution, k is the Boltzmann constant, T is the temperature, and ϵ is the permittivity of water. The solution to eq 2 for $V(\xi)$ intimately depends on appropriate boundary conditions. The negative PO_4^- surface of charge density $-\sigma$ launches an electric field toward the positive bicelle surface of magnitude $\mathrm{d}V(\xi = \xi_1)/\mathrm{d}\xi = \sigma a/\epsilon_b$, consistent with the $\mathrm{d}V(\xi = \xi_2)/\mathrm{d}\xi = -\sigma a/\epsilon_b$ field approaching the positive NMe_3^+ surface. The permittivity ϵ_b describes the electrical response of the region between the charged surfaces, as shown in Figure 2. Because the positive and negative charge density on the cationic and anionic surfaces are equal in the zwitterionic bicelles, the electric field at these surfaces can be used as boundary conditions to determine the potential $V(\xi{=}\xi_2)$ at the bicelle solution interface from the solution to LaPlace's equation or equivalently the solution to eq 2 with the right-hand side set to zero. The second boundary condition necessary to solve eq 2 in the free ion region between $\xi = \xi_2$ and $\xi = \xi_3$ is the zero electric field $\mathrm{d}V(\xi{=}\xi_3)/\mathrm{d}\xi = 0$ at the midpoint between bicelles.[12] The numerical solution to eq 2 for $V(\xi)$ in the region $\xi_2 < \xi < \xi_3$ with $V(\xi{=}\xi_2)$ set by the field developed between the PO_4^- and NMe_3^+ surfaces and $\mathrm{d}V(\xi{=}\xi_3)/\mathrm{d}\xi = 0$ is shown in Figure 3a for the usual parameter values of $e = 1.6 \times 10^{-19}$ C, $k = 1.38 \times 10^{-23}$ J/K, and $T =$ 300 K. In this case, the medium between the bicelle disks separated by $2d = 10$ nm contains $N = 1.95 \times 10^{26}/\mathrm{m}^3$ monovalent ions and water with a dielectric constant of $\epsilon/\epsilon_0 = 80$. The 234 mV value of the potential at the $\xi = \xi_2 = 0.16$ surface reflects the electric field developed in the phospholipid polar headgroup region, whereas the presence of ions between the bicelles permits the potential to substantially penetrate into the medium and ultimately decay to nearly zero at $\xi = \xi_3 = 0.39$. The solution for $V(\xi)$ shown in Figure 3a can be used to generate similar plots for the field gradient $\nabla^2V(\xi)$, the positive free charge density $\rho_+(\xi)$, and the negative free charge density $\rho_-(\xi)$ shown in Figure 3b−d, respectively.

The portion of the average field gradient for positive ions surrounding the bicelle that the NMR splitting measures is given by

$$\langle\nabla^2V\rangle = \frac{\int\left[\frac{\mathrm{d}}{\mathrm{d}\xi}(\xi^2+1)\frac{\mathrm{d}}{\mathrm{d}\xi}V(\xi)\right]\rho_+(\xi)\, d^{(2)}_{0,0}(\theta)\,\mathrm{d}\tau}{\int\rho_+(\xi)\,\mathrm{d}\tau} \qquad (3)$$

The Wigner reduced rotation matrix element $d^{(2)}_{0,0}(\theta)$ in eq 3 accounts for the change in principle axis direction for different positions around a bicelle. Equivalently, these factors track the direction of maximum field gradient at any point around the bicelle with reference to the center of the bicelle. Therefore, the $\theta = 0$ orientation is parallel to the symmetry axis of the bicelle and the $\theta = \pi/2$ orientation corresponds to the minor symmetry axis. If the bicelle were a sphere instead of an oblate spheroid the volume element $\mathrm{d}\tau$ in eq 3 would become $\mathrm{d}\tau = r^2 \sin\theta\,\mathrm{d}\theta\,\mathrm{d}\phi\,\mathrm{d}r$ and the integral over θ in eq 3 would be zero. However, in oblate spheroidal coordinates the volume element is $\mathrm{d}\tau = [a^3(\xi^2 - \cos^2\theta)\sin\theta\,\mathrm{d}\theta\,\mathrm{d}\phi\,\mathrm{d}\xi]/8$, a value that permits an analytical integration over θ in eq 3 and a simplification that reduces the average field gradient to

$$\langle\nabla^2V\rangle = \frac{-2\int_{\xi_2}^{\xi_3}\left[\frac{\mathrm{d}}{\mathrm{d}\xi}(\xi^2+1)\frac{\mathrm{d}}{\mathrm{d}\xi}V(\xi)\right]\rho_+(\xi)\,\mathrm{d}\xi}{5\int_{\xi_2}^{\xi_3}\rho_+(\xi)(3\xi^2-1)\,\mathrm{d}\xi} \qquad (4)$$

The numerical results shown in Figure 3 can be used in eq 4 to provide $\langle\nabla^2V\rangle = 1.95 \times 10^{16}\ \mathrm{V/m}^2$. Because the value of $\rho_+(\xi)$ in Figure 3c is nearly zero in the high field gradient region near the bicelle surface, the magnitude of the average gradient in eq 3 is smaller than the magnitude of the average gradient for negative ions. This inequivalence results because $\rho_-(\xi)$ in Figure 3d is larger than $\rho_+(\xi)$ in Figure 3c near the bicelle surface. The expression for $\langle\nabla^2V\rangle$ in eq 4 can be related to a value appropriate for a nucleus surrounded by electrons via the Sternheimer antishielding factor $(1 - \gamma_\infty)$.[19] Incorporating this correction into eq 4 allows the satellite splitting in eq 1 to be rewritten as

$$\Delta = -\frac{2(1-\gamma_\infty)eQ}{5h}\langle d^{(2)}_{0,0}(\beta)\rangle\langle\nabla^2V\rangle = \frac{(1-\gamma_\infty)eQ}{5h}\langle\nabla^2V\rangle \qquad (5)$$

where the average $\langle d^{(2)}_{0,0}(\beta)\rangle = -1/2$ is incorporated to indicate that the major symmetry axis of the bicelle is perpendicular to the applied magnetic field. Equivalently, all of the bicelles are considered to be aligned edge on in the magnetic field. Given that $Q = 1 \times 10^{-29}\ \mathrm{m}^{-2}$ and $h = 6.626 \times 10^{-34}$ J s apply, eq 5 along with the numerical result for $\langle\nabla^2V\rangle$ yields $\Delta = 600$ Hz when $(1 - \gamma_\infty) = 20.4$. A few parameter estimates have been used to match the theoretical value of Δ from eq 5 to experiment. The charge density N and distance between disks $2d$ are based

on a comparison of the total sample volume to the bicelle volume anticipated from the expression developed by Vold et al.[9] Given the success of this geometric equation in both NMR and X-ray studies of bicelle solutions, the values for N and $2d$ used here are most likely accurate to within an order of magnitude. Another estimate is in the $\sigma = 41\ \mu C/cm^2$ surface charge density used to establish the boundary conditions for eq 2 at $\xi = \xi_1$ and $\xi = \xi_2$. This value for σ was determined from the 38.9 Å^2 phospholipid headgroup area[18] and the number of phospholipid molecules and bicelles in solution. The calculation of Δ from $V(\xi)$ also uses $\epsilon_b/\epsilon_0 = \epsilon/\epsilon_0$. Although one would expect the dielectric constant in the polar headgroup region to be much different than that in solution, the extremely small size of the headgroup attenuates the effect of variations of ϵ_b/ϵ_0 on the ultimate void space potential. In fact, variations in ϵ_b/ϵ_0 between 1 and 80 provide $\langle\nabla^2 V\rangle$ values within a factor of 5 with respect to the $\epsilon_b/\epsilon_0 = \epsilon/\epsilon_0 = 80$ $\langle\nabla^2 V\rangle = 1.95 \times 10^{16}$ V/m^2 value mentioned above. Therefore, ϵ_b/ϵ_0 was taken to be 80 in all cases. The final estimate revolves around the Sternheimer factor of $(1 - \gamma_\infty) = 20.4$, a value that deviates by a factor of 4 from the ionic crystal value of 5.1. A similar discrepancy has also been noted in Pf1 solutions where $(1 - \gamma_\infty)$ values for ^{23}Na of 13.25 were reported.[14] It is not surprising that rigid ionic crystal Sternheimer values are not observed in liquid crystalline phase, as the charge distribution generating the shielding effect is not a point defect but rather a large macromolecular charged object—a physical situation where Sternheimer factors are not currently available and will be calculated in a future publication. Clearly the most suspicious parameter estimates in the comparison of the experimental $\Delta = 600$ Hz splitting in Figure 1 with the value determined from the solution of the nonlinear Poisson−Boltzmann equation shown in Figure 3a are the $(1 - \gamma_\infty) = 20.4$ Sternheimer factor and the $\epsilon/\epsilon_0 = 80$ dielectric constant for confined water. For this reason, the splitting Δ in eq 4 was recalculated using the Sternheimer factor of $(1 - \gamma_\infty) = 13.25$ observed for ^{23}Na in Pf1 solution.[14] To match theory to experiment the dielectric constant had to be lowered from $\epsilon/\epsilon_0 = 80$ to $\epsilon/\epsilon_0 = 18.5$. Such a decrease in dielectric constant is not unreasonable as the very small ≈5.3 zL volume void space between bicelles combined with high ionic strength can disrupt the hydrogen bonding network in bulk water, the property that leads to a high dielectric constant for water.[20]

Although the cell model of polyelectrolytes applied in the calculation of $V(\xi)$ reliably reproduces the experimental value for Δ while retaining physically meaningful parameter estimates, there are some very obvious limitations to this approach. For example, this model only considers ions confined to the region between bicelles and does not include the effects of ions in the polar headgroup region between the PO_4^- and NMe_3^+ surfaces or in the interior of the bicelle. Because the interior of the bicelle is nonpolar, it is not likely that any ions are located in this region. The effect of ions in the polar headgroup region on the splitting Δ can also be considered small as the fraction of ions in the void space is most likely much larger given the larger volume between bicelles and the fact that the positive NMe_3^+ surface occludes positive ions to the space between bicelles, as shown in Figure 3c. An additional limitation is the application of the cell model to the problem. In reality, each bicelle has a slight deviation from the perfect 26 nm diameter 4 nm thick idealized disk used here as well as some misalignment from the perfect edge on orientation in a magnetic field. A proper account of these effects necessarily includes the potential energy of interaction for all of the bicelles with each other and the ions in the entire sample. Because the size of such a computation is prohibitively large, the sample was considered to be composed of an ensemble of cells identical to the one shown in Figure 2. Within the cell model there is a further limitation worthy of comment. Both the inner and outer charged surfaces of the bicelle were taken to have a uniform $\sigma = 41\ \mu C/cm^2$ charge density. In reality these surfaces will not be uniformly charged, rather, a regular array of point charges corresponding to each of the ≈10,000 PO_4^- and NMe_3^+ groups will be present. The ≈6 Å spacing between these charges is important near the bicelle surface but can be considered a small effect given that the outer surface of the bicelle is both positively charged and that the effect of the point charges on the void space potential $V(\xi)$ is washed out very close to the bicelle surface by the free charge density at the ionic strength appropriate for this problem. Because the free positive charges are occluded from the zwitterionic surface as shown in Figure 3c, any substantial effect of the surface charge morphology will not be a major effect in the calculation of the average gradient for positive ions. It is important to realize, however, that if the average gradient for negative free ions were required, the surface charge morphology would most likely be important as virtually all of the negative charges are within 1 nm of the bicelle surface as shown in Figure 3d.

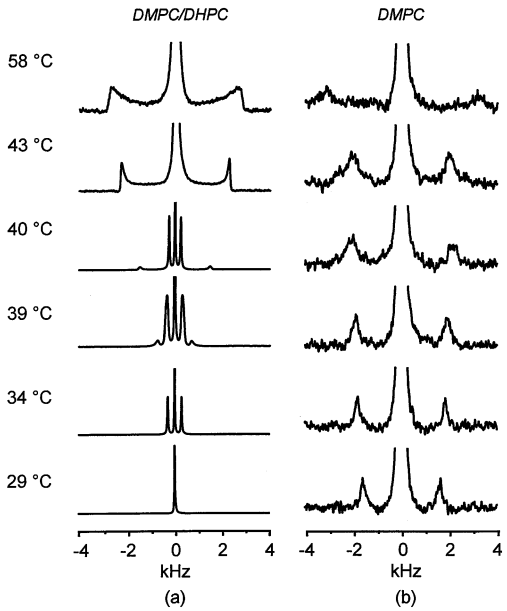

Figure 4. Temperature dependence of the ^{23}Na NMR data for 30 mM NaCl dissolved in a 40% w/v solution of DMPC/DHPC ($q = 3.25$) in (a) and a 40% w/v solution of pure DMPC in (b).

The Higher Temperature Phase

The ^{23}Na NMR spectra in Figure 4a for a 40% w/v $q = 3.25$ DMPC/DHPC solution display a strong dependence on temperature. At temperatures exceeding 40 °C the ^{23}Na NMR spectrum consists of a narrow center band and the satellite transitions display powder patterns indicative of a residual quadrupolar coupling that depends on the angle between the field gradient direction and the magnetic field. For comparison to lower temperature results, the position of the satellite frequency for these powder patterns is taken as the singularity corresponding to the orientation of $\nabla^2 V(\tau)$ perpendicular to the magnetic field. As the solution cools, the powder patterns disappear, the satellite transition splitting decreases, and an additional triplet with a smaller residual splitting develops. For example, at $T = 40$ °C the ^{23}Na NMR spectrum is a superposi-

tion of two triplets. As the known bicelle temperature region is accessed at $T = 34$ °C just one triplet is present, indicative of a highly homogeneous liquid crystalline phase that deteriorates by $T = 29$ °C. As a comparison, ^{23}Na NMR spectra for a 40% w/v DMPC solution were recorded over the same temperature region as shown in Figure 4b. Although the intensity of the satellite lines is insufficient to determine the presence of powder patterns, the large line widths at higher temperature suggest that the medium is disordered. In direct analogy to the DMPC/DHPC solutions the satellite transition splitting decreases as the temperature is lowered. The series of ^{23}Na NMR spectra in Figure 4a suggest that the binary DMPC/DHPC mixture forms at least two different temperature-dependent anisotropic phases. The well-known low-temperature bicelle phase was discussed in the previous section, but the higher temperature phase displaying powder-like satellite transition spectra has not yet been mentioned. Although disordered, the higher temperature phase does produce a larger field gradient than the bicelle phase at lower temperatures because the ^{23}Na satellite transition splitting is roughly 5−10 times larger at high temperatures. This assignment is consistent with previous ^{31}P and ^{2}H NMR spectra of high-temperature bicelle solutions where a new phase reportedly forms around 45 °C.[8,15] This new phase has also been identified by the growth of white flakes in a previously clear bicelle solution.[4,8] The presence of the particulate matter in solution most likely incorporates sodium cations and the instantaneous angle between the field gradient in these slowly tumbling flakes and the static magnetic field is what produces the high-temperature powder pattern.

Given the complexity and unknown nature of the electrostatic environment inside the particulate matter, calculation of the residual ^{23}Na splitting in terms of nuclear parameters is not possible for the phase at this time. However, some insight into the formation of the higher temperature phase can be obtained from the ^{23}Na NMR spectra in Figure 4 and the morphology of a bicelle. The DMPC rich bicelle has two parts, a long chained DMPC disklike bilayer capped on the edge with short-chained DHPC molecules.[9] The bicelle structure made with $q = 3-3.5$ is known to be stable in solution up to 40 °C. At higher temperatures thermal agitation begins forcing the DHPC molecules out of the edge of the bicelle and the remnant DMPC assembly is free to combine with other similar structures to form larger bilayers with occasionally interdigitated DHPC molecules, bilayers that ultimately grow to become visible flakes in solution.[8] At intermediate temperatures the DHPC population is likely partitioned between two phases. A fraction of the DHPC molecules cap the edge of bicelles whereas others become part of localized domains of DMPC rich bilayers. The consequence of this partitioning at intermediate temperatures is the coexistence of two phases, as suggested by the presence of overlapping triplets in the ^{23}Na NMR spectra in Figure 4a.

In contrast to the binary mixture of DMPC and DHPC, a solution containing only DMPC is not able to form bicelles. In fact the ^{23}Na NMR spectra in Figure 4b suggest that just one phase is present at temperatures up to 58 °C. The magnitude of the splittings observed at higher temperatures is comparable to those observed in the DMPC/DHPC binary solution shown in Figure 4a. A more detailed comparison of the outer and inner splittings observed in the DMPC/DHPC solution and the pure DMPC solution is provided in Figure 5. Here the circles track the ^{23}Na satellite splitting Δ for the higher temperature phase in the DMPC/DHPC solution as a function of temperature. Explicitly, the splitting corresponds to the outer satellites in Figure 4a. The splittings remain constant at ca. 5 kHz above

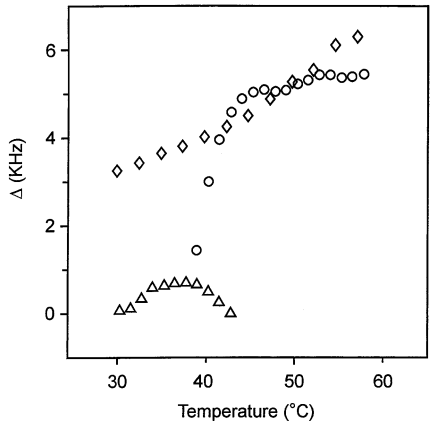

Figure 5. Summary of ^{23}Na satellite transition splittings for the 40% w/v DMPC/DHPC ($q = 3.25$) and 40% w/v DMPC solutions as a function of temperature. The ^{23}Na satellite transition splittings of the inner triplet for the binary DMPC/DHPC solution at temperatures below 40 °C are shown as triangles. The ^{23}Na outer satellite transition splittings in DMPC/DHPC solution at temperatures above 40 °C are marked with circles. The diamonds correspond to the ^{23}Na satellite transition splittings in the 40% w/v DMPC solution. Errors in both the temperature and splitting measurement are less than the marker size.

≈45 °C, indicating that this phase is stable up to at least 58 °C. The degeneration of this high-temperature phase occurs concomitant with the growth of the bicelle aggregates at lower temperatures. The triangles in Figure 5 track the ^{23}Na satellite transition splittings Δ for the bicelle phase in the DMPC/DHPC binary solution. Explicitly, these splittings correspond to the inner satellites in Figure 4a. The data summarized in Figure 5 indicate that the bicelle phase (triangles) is stable down to ≈29 °C where the solution undergoes a transformation to an isotropic gel-like phase.[8] Furthermore, Figure 5 suggests that the bicelle phase (triangles) and the high-temperature phase (circles) coexist between $T \approx 37$ °C and $T \approx 44$ °C. It is useful to compare these trends in DMPC/DHPC solution to the satellite splittings observed in the DMPC solution, shown as diamonds in Figure 5. The similarity in satellite splittings Δ at high temperatures between these two solutions suggests that the formation of DMPC aggregates in the DMPC/DHPC solution is likely. Clearly, this comparison (circles and diamonds) breaks down below $T \approx 45$ °C because of the formation of the bicelle phase at low temperature in the DMPC/DHPC binary system.

It is also important to comment on the satellite transition intensity in the DMPC solution in comparison to the binary DMPC/DHPC solution. Although the increased satellite transition splitting suggests increased order for pure DMPC at high temperature, the decreased transition intensity of these satellite lines at high temperature in comparison to low temperature in Figure 4b indicates that a smaller fraction of sodium cations are contained in this ordered particulate matter. Because both the DMPC/DHPC and DMPC solutions involve 40 % w/v lipids, the decreased satellite transition intensity in the DMPC solution suggests that the fraction of DMPC molecules participating in bilayer aggregates or equivalently flake formation in the DMPC/DHPC solution is greater than in the DMPC-only solution. This result implies that DHPC might play a vital role in the association of DMPC into macromolecular aggregates.

Conclusion

Quadrupolar ion NMR is used to probe the composition of an aqueous binary lipid mixture. The observed splittings for ^{23}Na and their temperature dependence provide information about the constitutional changes that occur in the solution as it

is cooled from 58 to 29 °C. Given the charged nature of both the bicelle and the sodium cation, it is not surprising that the method is sensitive to effects different from those for the ^{2}H NMR spectrum of D_2O in the void space between bicelles. For example, ^{2}H NMR of D_2O is not able to monitor the formation of the high-temperature phase.[8] In fact, on the basis of just the ^{2}H NMR of D_2O alone, one would expect that the binary DMPC/DHPC solution is isotropic and not oriented at high temperatures, in striking disagreement with the ^{23}Na results reported here. It is not surprising that the solution to the Poisson−Boltzmann equation in oblate spheroidal coordinates reliably estimates the residual quadrupolar coupling $\Delta = 600$ Hz in the bicelle phase given the 41 μC/cm^2 surface charge on the bicelle. This approach is, however, limited by the lack of available Sternheimer shielding parameters[14,19] for noncrystalline ionic systems. Future work will include the determination of these values in charged liquid crystalline media. In closing, it is interesting to note that ^{23}Na residual quadrupolar splittings were not reported in DMPC/DHPC solutions in a previous study.[21] The lack of splittings in this system is most likely due to a combination of low magnetic field and lower bicelle concentration, conditions where the magnetic ordering of the bicelles is lower and consequently, large void space potentials that are capable of supporting a reasonable ion atmosphere do not develop.

Acknowledgment. Support from the NSF under grant number CHE-9984654 is gratefully acknowledged. M.P.A. is a David and Lucile Packard Foundation and Alfred P. Sloan Foundation Fellow.

References and Notes

(1) Hansen, M. R.; Mueller, L.; Pardi, A. *Nature Struct. Biol.* **1998**, *5*, 1065.

(2) Kroenig, B. W.; Hu, J.; Ottiger, M.; Bose, S.; Hendler, R. W.; Bax, A. *J. Am. Chem. Soc.* **1999**, *121*, 1385.

(3) Creuzet, F.; McDermott, A.; Gebhard, R.; Van Der Hoef, K.; Spijker-Assink, M. B.; Herzfeld, J.; Lugtenburg, J.; Levitt, M. H.; Griffin, R. G. *Nature* **1991**, *251*, 783.

(4) Sanders, C. R., II; Landis, G. C. *Biochemistry* **1995**, *34*, 4030.

(5) Tjandra, N.; Tate, S.; Ono, A.; Kainosho, M.; Bax, A. *J. Am. Chem. Soc.* **2000**, *122*, 6190.

(6) Ottiger, M.; Bax, A. *J. Biomol. NMR* **1999**, *13*, 187.

(7) Vold, R. R.; Prosser, R. S.; Deese, A. J. *J. Biomol. NMR* **1997**, *9*, 329.

(8) Ottiger, M.; Bax, A. *J. Biomol. NMR* **1998**, *12*, 361.

(9) Vold, R. R.; Prosser, R. S. *J. Magn. Reson.* **1996**, *113*, 267.

(10) Wennerström, H.; Lindman, B.; Lindblom, G.; Tiddy, G. J. T. *J. Chem. Soc., Faraday Trans.* **1979**, *75*, 663.

(11) Wennerström, H.; Lindman, B.; Engström, S.; Lindblom, G.; Tiddy, G. J. T. In *Magnetic Resonance in Colloid and Interface Science*; Fraissard J. P., Resing, H. A., Eds.; Reidel: Boston, 1980; p 609.

(12) Van der Klink, J. J.; Zuiderweg, L. H.; Leyte, J. C. *J. Chem. Phys.* **1974**, *60*, 2391.

(13) Fuoss, R. M.; Katchalsky, A.; Lifson, S. *Proc. Natl. Acad. Sci.* **1951**, *37*, 579.

(14) Vyas, S.; Hernandez, C.; Augustine, M. P. *J. Chem. Phys.* **2002**, *116*, 7109.

(15) Sanders, C. R., II; Schwonek, J. P. *Biochemistry* **1992**, *31*, 8898.

(16) Morse, P. M.; Feshbach, H. *Methods of Theoretical Physics*; McGraw-Hill: New York, 1953; Vol. 2, p 1292.

(17) Engström, S.; Wennerström, H. *J. Phys. Chem.* **1978**, *82*, 2711.

(18) Hauser, H.; Pascher, I.; Pearson, R. H.; Sundell, S. *Biochim. Biophys. Acta* **1981**, *650*, 21.

(19) Sternheimer, R. M.; Peierls, R. F. *Phys. Rev. A* **1971**, *3*, 837.

(20) Pottel, R. In *Chemical Physics of Ionic Solutions*; Conway, B. E., Barradas, R. G., Eds.; John Wiley & Sons: New York, 1966; p 583.

(21) Cho, G.; Fung, B. M.; Reddy, V. B. *J. Am. Chem. Soc.* **2001**, *123*, 1537.